The limited contribution from outer core dynamics to global deformations at the Earth's surface

N Gillet, M Dumberry, Séverine Rosat

submitted to *Geophys. J. Int.*

The limited contribution from outer core dynamics to global deformations at the Earth's surface

N. Gillet[1], M. Dumberry[2] & S. Rosat[3]

[1] *Univ. Grenoble Alpes, Univ. Savoie Mont Blanc, CNRS, IRD, IFSTTAR, ISTerre, F-38000 Grenoble, France*

[2] *Department of Physics, University of Alberta, Edmonton T6G 2E1, Canada*

[3] *Institut de Physique du Globe de Strasbourg, UMR 7516, CNRS/Universit de Strasbourg, 67084 France*

SUMMARY

Planetary scale interannual deformations of the Earth's surface, of millimetric amplitude, have recently been related to both geomagnetic field changes and motion within the fluid outer core. We calculate the temporal variations of the dynamical pressure at the surface of the core associated with core flow models inverted from geomagnetic observations. From these we compute predictions of the changes in Earth's topography in response to elastic deformations in the mantle. We show that at decadal periods, the predicted changes in Earth's topography are at most of the order of 0.3 mm. Focused at interannual periods between 4 and 9.5 yr, the predicted topography variations are smaller than 0.05 mm, at least an order of magnitude smaller than the reported observations. These amplitudes are only weakly sensitive to the choice of hypothesis used to reconstruct fluid motions at the core surface. We conclude that surface deformations induced by dynamical pressure changes in the core are below the detection level at present-day. Alternative geophysical sources must be sought to explain the observed millimetric interannual variations of the planetary scale topography, and its associated gravity variations. We currently see no justification for a physical relationship between interannual fluctuations of the geomagnetic

field and of Earth's observed deformations. We conjecture that the largest gravity signal of core origin is potentially associated with decadal longitudinal oscillations of the inner core. It might be detectable as longer series will become available.

Key words: surface deformations – core dynamics – elastic mantle – geomagnetic secular variation

1 GEOPHYSICAL MOTIVATIONS

Two recent studies (Ding & Chao 2018; Watkins et al. 2018) have put to the fore the presence of a planetary scale $\sim$ 1 mm amplitude signal in the surface displacement recorded by the Global Positioning System (GPS) network, each with a period of approximately 6 yr. In both of these studies, a possible connection to flows in the Earth's core was proposed. The study of Ding & Chao (2018) suggests that a non-axisymmetric (or non-zonal) spherical harmonic degree 2, order 2 signal in GPS data is propagating westward and potentially linked with a similar signal in geomagnetic observatory data. The study of Watkins et al. (2018) argues for a connection between axisymmetric (or zonal) core flows and surface vertical displacement data. These scenarios are potentially appealing since it has been shown that zonal azimuthal fluid motions in the outer core can explain the observed changes in the length-of-day (LOD) at a period of 6 yr (Gillet et al. 2010, 2015b). Indeed, in both Ding & Chao (2018) and Watkins et al. (2018), the role of core flows was suggested in part on the basis of this connection with the 6 yr LOD changes.

A natural link between core flows and surface deformation may be found through elastic deformations of Earth's mantle. In order to preserve its mechanical equilibrium, any force applied on the mantle must be accompanied by small elastic deformations (e.g. Alterman et al. 1959; Crossley 1975). Changes in the pressure field at the core-mantle boundary (CMB), connected to core flow variations, should entrain elastic deformations in the whole Earth, including vertical and lateral displacements at the Earth's surface (Fang et al. 1996; Dumberry & Bloxham 2004; Greff-Lefftz et al. 2004, the latter two hereafter referred to as DB04 and GPL04 respectively). Likewise, changes in the density field within the volume of the core perturb the global gravity field and are also accompanied by surface displacements (e.g. Dumberry 2010).

The prediction made by GPL04 suggests that, indeed, surface displacements induced by core flows are of the order of 1 mm (see their Figure 4). However, this applies for the steady or slowly changing part of core flows (decades to centuries). For low spherical harmonic degrees, the temporally changing part of core flows is typically an order of magnitude weaker than the steady part (e.g. Bloxham 1992; Gillet et al. 2015b). Hence, time-dependent changes in surface topography connected to outer core

dynamics should be closer 0.1 mm, as was shown in DB04 though their results were limited to zonal deformations. This is an order of magnitude smaller than those suggested by Watkins et al. (2018) to occur at sub-decadal periods, and thus seemingly at odds with their results. Yet, in core flow models inverted from geomagnetic data, non-zonal flows have a significantly larger amplitude than zonal flows at interannual periods (see Gillet et al. 2015b, 2019; Kloss & Finlay 2019). Thus there is an interest to investigate in more details whether interannual core flows could be connected to a 6 yr surface deformation, in particular to address the suggestion made by Ding & Chao (2018).

If a connection between core flows and surface deformation can be firmly established, this opens the possibility of further constraining the dynamics in the outer core from geodetic measurements. Moreover, it could ensure that a part of the observed surface deformation is not wrongly attributed to processes in the atmosphere, oceans or continental hydrology. These considerations provide the underlying motivation for our study.

Our goal is to address the following two main questions. First, we wish to provide an estimate of the pressure anomaly at the core-mantle boundary (CMB) associated with core surface flow models. Second, on the basis of this pressure change, we wish to compute an associated prediction of the deformation at the Earth's surface. We can thereby asses whether core flows can be responsible for the changes of the order of 1 mm at a period of 6 yr in the low harmonic degree topography reported by Ding & Chao (2018) and Watkins et al. (2018). Theoretical aspects for each of these two questions are presented in §2 and §3, respectively. We present in §4 results obtained from recent core flow models, and discuss in §5 their geophysical implications.

2 PRESSURE FIELD AT THE CMB

We consider below two orthonormal frames: $(\mathbf{1}_r, \mathbf{1}_\theta, \mathbf{1}_\phi)$ in spherical coordinates, and $(\mathbf{1}_s, \mathbf{1}_\phi, \mathbf{1}_z)$ in cylindrical polar coordinates, in which r is the distance from the Earth's centre, s is the (cylindrical) radial distance from the rotation axis, z is position in the axial direction, θ is colatitude and ϕ is longitude.

In order to retrieve the pressure exerted on the CMB (of radius $r = c$) from core flows, one needs to consider the balance of forces. One instance of such balance that has been widely used is the tangentially geostrophic hypothesis (TG, see Le Mouël 1984), where one assumes an equilibrium between the Coriolis force and the pressure gradient near the CMB:

$$2\rho\Omega\mathbf{1}_z \times \mathbf{u} = -\nabla p\,. \tag{1}$$

Here, $\mathbf{u}$ is the fluid velocity, p the modified pressure (i.e. including the centrifugal force), ρ the fluid density and Ω the Earth's rotation rate. The horizontal component $\mathbf{u}_h = u_\theta\mathbf{1}_\theta + u_\phi\mathbf{1}_\phi$ of TG flows

must obey the following constraint at the core surface,

$$\nabla_h \cdot (\mathbf{u}_h \cos\theta) = 0\,, \tag{2}$$

and are connected to the pressure field via (Le Mouël et al. 1985)

$$\mathbf{u}_h = \frac{\mathbf{1}_r \times \nabla_h p}{2\rho\Omega\cos\theta}\,, \tag{3}$$

with ∇_h the horizontal gradient.

We can write the pressure field at the CMB as an expansion of surface spherical harmonics with coefficients $p_n^{mc,s}$,

$$p(\theta,\phi) = \sum_{n=1}^{N}\left[p_n^0 P_n^0(\cos\theta) + \sum_{m=1}^{n}\left[p_n^{mc}\cos(m\phi) + p_n^{ms}\sin(m\phi)\right]P_n^m(\cos\theta)\right]\,, \tag{4}$$

where P_n^m are the Schmidt semi-normalized associated Legendre polynomials of degree n and order m, and N is the truncation level. The flow at the core surface is expanded similarly in terms of toroidal and poloidal coefficients $(t_n^{mc,s}, s_n^{mc,s})$, and can be reconstructed from the observed geomagnetic secular variation (see Holme 2015). Using Equation (3), the pressure coefficients is directly connected to flow coefficients $t_n^{mc,s}$, $s_n^{mc,s}$ – see Gire & Le Mouël (1990), hereafter referred to as GL90. In this TG framework, for $n \geq 2$, the zonal pressure coefficients p_n^0 are related to the zonal toroidal coefficients $t_{n\pm1}^0$, while the non-zonal coefficients $p_n^{m\neq0}$ are related to the non-zonal poloidal coefficients s_n^m and $s_{n\pm2}^m$, with linear relations of the form

$$\text{for } m=0: \quad p_n^0 = K\left(\alpha_n^- t_{n-1}^0 + \alpha_n^+ t_{n+1}^0\right)\,, \tag{5a}$$

$$\text{for } m\neq0: \quad p_n^{mc} = K\left(\beta_{nm}^- s_{n-2}^{ms} + \beta_{nm} s_n^{ms} + \beta_{nm}^+ s_{n+2}^{ms}\right)\,, \tag{5b}$$

$$p_n^{ms} = -K\left(\beta_{nm}^- s_{n-2}^{mc} + \beta_{nm} s_n^{mc} + \beta_{nm}^+ s_{n+2}^{mc}\right)\,, \tag{5c}$$

where $K = 2c\rho\Omega$ and the α_n's and β_{nm}'s are numerical factors that depend on n and m.

An order of magnitude estimate of the pressure at the CMB based on Equation (1) is $p = 2\rho\Omega UL \sim 700$ Pa (e.g. GPL04, Dumberry 2010) when using a length-scale $L \sim 1000$ km, a typical core flow magnitude of $U \sim 5\times10^{-4}$ m s^{-1}, and parameters from Table 2. This estimate is appropriate when considering the steady or slow (centennial) changes in core flows. Flows that vary over decades or shorter periods are approximately 5 to 10 times weaker (e.g. Figure 12 of Gillet et al. 2015b), and using $U \sim 5\times10^{-5}$ m s^{-1} instead, one gets a typical pressure variation of $p' \sim 70$ Pa. In comparison, the magnetic pressure at the CMB, $p_M = B^2/(2\mu)$, with B the magnetic field intensity and μ the magnetic permeability of free space, is much smaller. Changes in B are at most 1 mT (e.g. Finlay & Jackson 2003), so that $p_M < 1$ Pa. Note that this estimate applies again for slow (centennial) changes; much smaller magnetic pressure variations of the order of $p'_M = BB'/(2\mu) < 10^{-2}$

Pa are expected for interannual fluctuations of the magnetic field $B' \sim BUT/L \sim 10^{-2}$ mT at a period $T = 6$ yr. This is 3 orders of magnitude smaller than the geostrophic pressure p' and can be neglected. The slow changes in the kinetic pressure is $p_K = \rho U^2/2 \sim 10^{-3}$ Pa, its interannual change is $p'_K \sim 10^{-5}$ Pa and can also be safely neglected.

The closed form relationships of Equation (5) are convenient because they allow one to compute the pressure at the CMB directly from a model of the flow at the surface of the core. However, it is not exact if the flow at the CMB does not strictly obey the TG constraint. Indeed, the assumption of Equation (2) is inaccurate if the Coriolis force dominates in the whole volume of the core. If this is the case, core flows parallel to the equatorial plane are to first order invariant along the rotation axis and their geometry is instead governed by the divergence-free quasi-geostrophic (QG) condition.

For QG flows (or helical flows, see Amit & Olson 2004; Pais & Jault 2008), the constraint of Equation (2) is replaced by

$$\nabla_h \cdot \left(\mathbf{u} \cos^2 \theta \right) = 0 \,, \tag{6}$$

with the additional condition that flows must be symmetric about the equator outside the polar caps that encapsulates the cylinder tangent to the inner core and aligned with $\mathbf{1}_z$ (the so-called 'tangent cylinder'):

$$u_\phi(\theta, \phi) = u_\phi(\pi - \theta, \phi) \;,\; u_\theta(\theta, \phi) = -u_\theta(\pi - \theta, \phi) \,. \tag{7}$$

QG flows in the whole of the outer core volume (outside the tangent cylinder) can be defined by a stream function $\psi(s, \phi)$ that depends only on s and ϕ (e.g. Schaeffer & Cardin 2005; Labbé et al. 2015):

$$\mathbf{u}(s, \phi, z) = \frac{1}{H} \nabla \times (\psi \mathbf{1}_z) - \frac{z}{H^3} \frac{\partial \psi}{\partial \phi} \mathbf{1}_z \,, \tag{8}$$

where $H = (c^2 - s^2)^{1/2}$ is the half-height of geostrophic columns. The second term on the right-hand side of Equation (8), linear in the z coordinate, represents an axial flow necessary to conserve mass and to obey the no-penetration condition at the CMB. In contrast to Equation (3), the stream function ψ in Equation (8) cannot be directly related to the pressure. With the flow defined by Equation (8), extra forces (e.g. Lorentz, buoyancy) that are neglected in the geostrophic equilibrium of Equation (1) necessarily enter the force balance at play. Indeed, when taking the curl of Equation (1), the right-hand side equals zero; however, with a flow defined by Equation (8) the curl of the Coriolis term is not null:

$$\nabla \times (2\rho\Omega \mathbf{1}_z \times \mathbf{u}) = 2\rho\Omega \frac{1}{H^3} \frac{\partial \psi}{\partial \phi} \mathbf{1}_z \neq \mathbf{0} \,. \tag{9}$$

Without an explicit knowledge of these other forces, it is not possible to calculate exactly the pressure at the CMB within the QG approximation (see also section 2.3 of Gerick et al. 2020). In their study of QG eigen modes (and of the associated pressure torque) within an ellipsoidal mantle in the presence

of a magnetic field, Gerick et al. alleviate this difficulty by using a two-dimensional representation (similar to Equation 8) for the magnetic field perturbation. This way they can represent in the whole domain the Lorentz force associated with the modes. Knowing the forces at stake, they can access to the pressure.

The example above illustrates that, unless a core flow model is built to satisfy the TG constraint, the pressure cannot be retrieved in a straightforward manner on the basis of kinematic core flows alone. Nevertheless, the order of magnitude estimate of the pressure that we have presented on the basis of geostrophy should remain correct to first order since the Coriolis force is expected to play a dominant role in the momentum balance. To illustrate this, at a period of $T = 6$ yr the Rossby number, which measures the ratio between the magnitudes of inertia (U/T) over the Coriolis force, is $Ro = 1/(2\Omega T) \simeq 2 \times 10^{-4} \ll 1$. Likewise, the Lehnert number $Le = B/\sqrt{\rho\mu}\Omega L$, which measures the ratio of the inertial waves time-scale $1/\Omega$ to the Alfvén (i.e. magnetic) time $T_A = L\sqrt{\rho\mu}/B$, is of the same order (here B is the magnetic field intensity deep in the core). Buoyancy forces may be proportionally more important, especially if the top of the core is strongly stratified (e.g. Buffett 2014), but they act in the radial direction and do not affect the first order horizontal geostrophic balance of Equation (1).

The strategy that we follow here is to calculate the pressure from Equation (5) for a few different flow models. Some of these models are built to obey the TG constraint exactly, in which case using Equation (5) is appropriate. For flow models not built to obey the TG constraint, we can evaluate the pressure either by using the flow model coefficients directly in Equation (5), or in a two step process where we first project the flow model onto a TG basis (for details, see e.g. Jackson 1997; Gillet et al. 2009), and then evaluate the pressure by Equation (5). The difference in the pressure between these two cases should be illustrative of the error in the recovery of the pressure on the basis of Equation (5). As we will show, this error is typically not greater than the pressure difference originating from different flow models.

3 SURFACE DEFORMATIONS

The pressure on the CMB imposed by core flows perturb the mechanical equilibrium of the mantle. This leads to small elastic deformations in the whole Earth, including at the Earth's surface. The connection between a pressure at the CMB and the resulting deformation at the surface can be cast into a formalism of Love numbers (Love 1909). Here, we focus on the vertical component of the deformation at the surface, which can be expanded as in Equation (4) with a set of coefficients $d_n^{mc,s}$. Following DB04 and GPL04, the coefficients $d_n^{mc,s}$ are connected to the pressure coefficients at the

CMB $p_n^{mc,s}$ by a Love numbers h_n,

$$\text{for } (n,m) \neq (2,0)\text{: } d_n^{mc,s} = \frac{h_n}{\overline{\rho} g} p_n^{mc,s} \,, \tag{10}$$

with g the gravity at the surface and $\overline{\rho}$ is the mean density of Earth. The numerical values of the Love numbers h_n depend on the density and elastic structure of a chosen Earth model. They were calculated in DB04 and GPL04 based on PREM (Dziewonski & Anderson 1981); their low spherical harmonic degree values are given in Table 1. Note that h_n were also computed in the earlier study of Fang et al. (1996), with values larger than those presented in Table 1. However, as noted in DB04, their calculation failed to account for the deformation of equipotential surfaces within the core.

In addition to the contribution from p_2^0, the zonal d_2^0 coefficients also includes a contribution from a change in Earth's rotation rate which we denote d_2^Ω,

$$d_2^0 = \frac{h_2}{\overline{\rho} g} p_2^0 - d_2^\Omega \,. \tag{11}$$

The second term in the r.h.s. of (11) comes from the exchange of angular momentum between the core and the mantle (see DB04): d_2^Ω results from the elastic deformation due to a perturbation in the rotation of the mantle (thus in its centrifugal potential). Using the TG rules of GL90, p_2^0 depends on the toroidal flow coefficients t_1^0 and t_3^0:

$$p_2^0 = -\frac{2\rho\Omega c}{3}\left(t_1^0 + \frac{12}{7} t_3^0\right) . \tag{12}$$

Likewise, d_2^Ω depends on the same flow coefficients (see DB04), and can be written as

$$d_2^\Omega = -\frac{2h_2^\Omega}{3g}\frac{\Omega a^2}{c}\frac{I_c}{I_m}\left(t_1^0 + \frac{12}{7} t_3^0\right) , \tag{13}$$

where a is the Earth radius, I_c and I_m are the moments of inertia of the core and mantle, respectively, and h_2^Ω is a Love number characterizing the vertical surface displacement in response to a unitary centrifugal potential. Its numerical value, based on PREM (Dziewonski & Anderson 1981), is $h_2^\Omega = 0.4769$ (DB04). Equation (11) can thus be written as

$$d_2^0 = \frac{h_2}{\overline{\rho} g} p_2^0 \,(1-\zeta) \,, \tag{14}$$

with

$$\zeta = \frac{h_2^\Omega}{h_2}\frac{\overline{\rho}}{\rho}\frac{I_c}{I_m}\left(\frac{a}{c}\right)^2 . \tag{15}$$

For the numerical values given in Table 2, we obtain $\zeta = 0.447$.

We do not compute surface displacement of degree 1. This would require the knowledge of the Love number h_1, which was not computed in DB04 and GPL04 as it represents a particular case of elastic deformation connected to the conservation of the centre of mass (see Greff-Lefftz & Legros 1997, 2007).

Table 1. Love numbers computed as in DB04 based on PREM Earth model (Dziewonski & Anderson 1981)

$h_2^\Omega = 4.769 \cdot 10^{-1}$		
$h_2 = 2.302 \times 10^{-1}$	$h_5 = 2.598 \times 10^{-2}$	$h_8 = 4.013 \times 10^{-3}$
$h_3 = 1.065 \times 10^{-1}$	$h_6 = 1.366 \times 10^{-2}$	$h_9 = 2.204 \times 10^{-3}$
$h_4 = 5.135 \times 10^{-2}$	$h_7 = 7.357 \times 10^{-3}$	$h_{10} = 1.215 \times 10^{-3}$

4 RESULTS

4.1 Core flow models

We use below several core surface flow models from previous studies. From these we calculate the pressure variations at the CMB, and subsequently the vertical deformations at the Earth's surface following the formalism described in Sections §2–3. These core flow models have been inverted, using various algorithms, from models of the geomagnetic field valid outside the electrically conducting core (at radii $r \geq c$). As such they do fit changes in the geomagnetic field recorded above the Earth's surface. They have been constructed based on different topological constraints, either obeying strictly the TG constraint (2) – with or without the equatorial symmetry constraint (7) –, satisfying the QG conditions (6-7), or under alternative constraints from dynamo simulations.

Instead of imposing purely the QG constraint, a few studies (e.g. Pais & Jault 2008; Gillet et al. 2009) have considered symmetric TG flows, imposing together constraints (2) and (7). Mathematically, this tends to be similar to the QG constraint although only for small vortices that are far from the equatorial region. However, for planetary scale features such flows do not satisfy the solenoidal

name	symbol	value	units
Earth radius	a	6.371×10^6	m
outer core radius	c	3.485×10^6	m
Earth rotation rate	Ω	7.292×10^{-5}	s^{-1}
outer core density at the CMB	ρ	9.903×10^3	$\mathrm{kg\ m}^{-3}$
mean density of Earth	$\overline{\rho}$	5.515×10^3	$\mathrm{kg\ m}^{-3}$
core moment of inertia	I_c	0.908×10^{37}	$\mathrm{kg\ m}^2$
mantle moment of inertia	I_m	7.129×10^{37}	$\mathrm{kg\ m}^2$
gravitational acceleration at the surface	g	9.820	$\mathrm{m\ s}^{-2}$
Mass of Earth	M	5.972×10^{24}	kg
gravitational constant	G	6.674×10^{-11}	$\mathrm{m}^3\ \mathrm{kg}^{-1}\ \mathrm{s}^{-2}$

Table 2. Geophysical parameters used to estimate surface deformations and Stokes coefficients.

constraint $\nabla \cdot \mathbf{u} = 0$. Estimates of the large length-scale pressure field thus potentially differ for flows calculated with the TG and QG constraints.

In a different approach, dynamo norms have been considered to reduce non-uniqueness issues for the core flow inverse problem (by calculating a priori cross-covariances from geodynamo runs, e.g. Fournier et al. 2011; Barrois et al. 2017; Gillet et al. 2019). Since the force balance is accessible in dynamo simulations (e.g. Aubert 2018), this avenue is potentially interesting in order to estimate the pressure, provided one can access efficiently the dynamical equilibrium below the CMB based solely on observations of the magnetic variations outside the conducting core. This is outside the scope of the present study. Nevertheless, dynamo norms implicitely impose (in a weak form) the domination of the Coriolis force in the momentum balance as observed in dynamo simulations (Aubert et al. 2017). Hence we do not expect the pressure to be largely different from that estimated on the basis of other approaches.

The specific flow models that we use here are:

- The flow model 'GJF15_QG' covers the time interval 1940-2010. It is inverted from the field model COV-OBS (a spatio-temporal interpolation of surveys, observatory and satellite data, see Gillet et al. 2013) under the QG constraint of Equations (6-7), using a stochastic temporal prior imposed with a weak formalism (see Gillet et al. 2015b).

- The flow model 'GHA19_DN' covers the time interval 1880-2015. It is inverted from the field model COV-OBS.x1 (an extension of COV-OBS, see Gillet et al. 2015a) under a dynamo norm, using a stochastic augmented state Kalman filter (see Gillet et al. 2019).

- The flow models 'GSJ11_TGsym' and 'GSJ11_TG' cover the time interval 1880-2008. They are inverted (from the field model described in Appendix C of Gillet et al. 2011, also based on surveys, observatory and satellite data) under the TG constraint of Equation (2) with and without, respectively, the equatorial symmetry constraint of Equation (7) (see Gillet et al. 2011).

Each of these flow models corresponds to the mean over an ensemble of models, the spread within each ensemble resulting primarily from the unresolved magnetic induction at small length-scales (see the above references for methodological details). For the purpose of the present study, and for the sake of simplicity, it is sufficient to only consider these ensemble averages. The main characteristics of the above flow models are summarized in Table 3.

name	constraint	time interval	reference
GHA19_DN	dynamo norm	1880–2015	Gillet et al. (2019)
GJF15_QG	QG: eq. (6) and (7)	1940–2010	Gillet et al. (2015b)
GSJ11_TG	TG: eq. (2)	1880–2008	Gillet et al. (2011)
GSJ11_TGsym	TG: eq. (2) and (7)	1880–2008	Gillet et al. (2011)

Table 3. Main characteristics of the core surface flow models.

4.2 CMB pressure and deformations at the Earth surface

4.2.1 Changes on decadal time-scales

We define, for $n \geq 2$, the spatial spectra for the time-dependent part of the pressure at the CMB and of the vertical deformations at the Earth's surface:

$$S_d(n,t) = \frac{1}{2n+1}\left[\tilde{d}_n^0(t)^2 + \sum_{m=1}^{n}\left(\tilde{d}_n^{mc}(t)^2 + \tilde{d}_n^{ms}(t)^2\right)\right], \tag{16}$$

$$S_p(n,t) = \frac{1}{2n+1}\left[\tilde{p}_n^0(t)^2 + \sum_{m=1}^{n}\left(\tilde{p}_n^{mc}(t)^2 + \tilde{p}_n^{ms}(t)^2\right)\right]. \tag{17}$$

We use the notation $\tilde{x}(t) = x(t) - \overline{x}$, where overlines denote for each model the time-average over a reference period $[t_s, t_e] = [1940, 2000]$. The prefactor $\frac{1}{2n+1}$ originates from the normalization of the associated Legendre polynomials. Despite important differences in the assumptions and methods used to build each flow model, their spectra $S_d(n,t)$ time averaged over $[t_s, t_e]$ are broadly similar (Figure 1, top). The amplitude falls rapidly with harmonic degree n, approximately as $\exp(-0.65n)$. This occurs primarily because of the sharp decrease of the h_n with n (see Table 1). Indeed, the corresponding time averaged pressure spectra (Figure 1, bottom) show little dependence with n, consistent with the rather flat spatial spectrum of core surface motions (Gillet et al. 2015b; Baerenzung et al. 2016). Note that the projection onto the geostrophic basis of QG flows reduces (by about 30-40%) the estimate of the pressure at the largest length-scales. The r.m.s. of the predicted amplitude of surface deformations is below 0.1 mm for harmonic degrees larger than $n = 4$. Given the present-day resolution of GPS observations (e.g. Teferle et al. 2008), there is no need to consider surface displacements at harmonic degrees larger than degree 4.

The time series of the pressure at the CMB and vertical deformation at the surface for the zonal coefficients of degree 2 and 4 are shown in Figure 2 (left). Decadal variations in pressure are of the order of 50 to 100 Pa, compatible with our above estimates; surface deformations are between 0.1-0.3 mm, consistent with the results of DB04 (see their Figure 12). There is a large degree of coherence between the temporal variations predicted from the different flow models. This is to be expected: the zonal flow coefficients t_n^0 tend to be similar within the several flow models as they

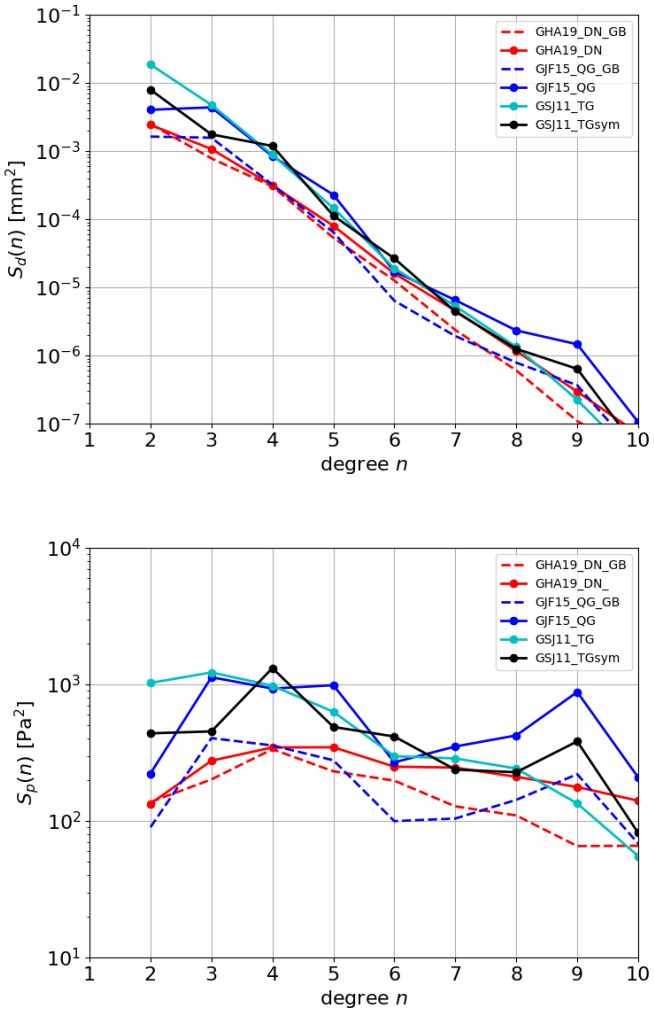

Figure 1. Spectra $S_d(n)$ (top, in mm^2) and $S_p(n)$ (bottom, in Pa^2), time averaged over 1940–2000, obtained for the models listed in Table 3. The extension '_GB' indicates a projection of the flow model onto a TG basis prior to using Equation (5).

are left unconstrained by the conditions of Equations (2) and (6) for the TG and QG assumptions, respectively.

Figure 3 (left) shows the time series for the non-zonal coefficients p_2^{2s} and p_3^{1c} and associated surface deformation coefficients d_2^{2s} and d_3^{1c}. Again note that the amplitude of the deformation is much smaller than 1 mm. Unlike for the toroidal zonal flow coefficients, the non-zonal flow coefficients are noticeably affected by the choice of the TG or QG constraint: the coefficients t_n^m are linked to $s_{s\pm1}^m$ (resp. $s_{s\pm2}^m$) in the TG (resp. QG) assumption. This is most evident for the recent changes in $d_2^{2,s}(t)$. Yet, despite these differences, some degree of coherence between the several flow models remains,

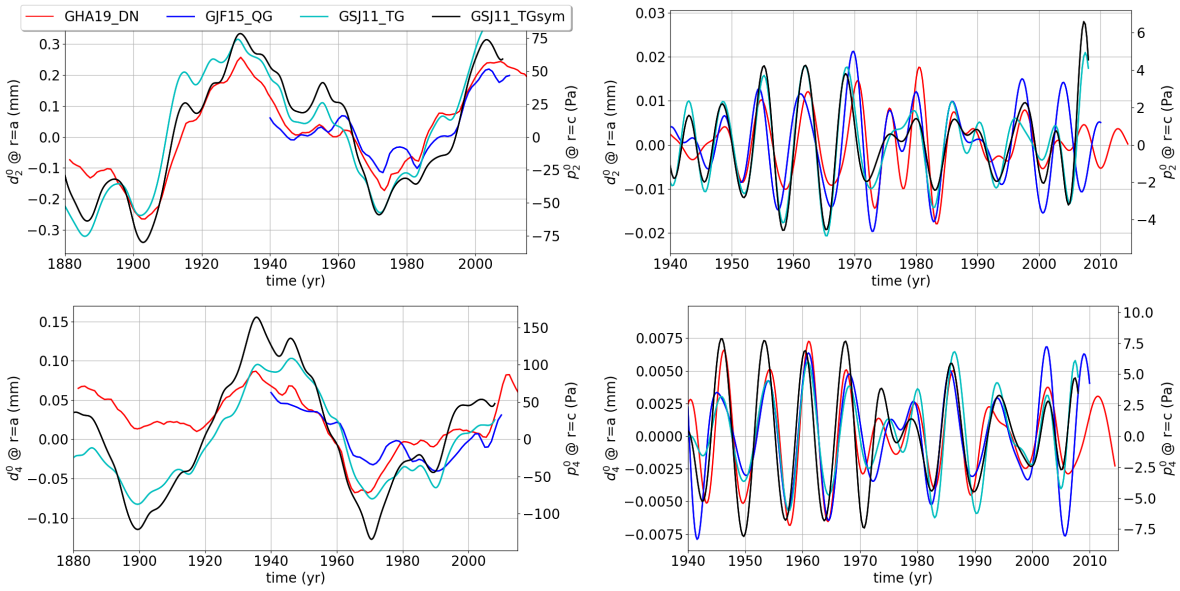

Figure 2. Left: time series of the vertical deformation at the Earth's surface (left y-axis, in mm) for zonal coefficients d_2^0 (top) and d_4^0 (bottom), for the different flow models listed in Table 3. The change in the associated coefficients of pressure at the CMB p_2^0 and p_4^0 is indicated on the right y-axis (in Pa). The extension '_GB' indicates a projection of the flow model onto a TG basis prior to using Equation (5). Right: time series band-pass filtered between 4 and 9.5 yr. The legend is common to all 4 panels.

though perhaps not as strongly as in Figure (2). The amplitude of the decadal changes in the low degree non-zonal coefficients of the CMB pressure are approximately 50 to 100 Pa.

For the two flow models that do not naturally obey the TG constraint (GHA19_DN and GJF15_QG), the pressure perturbations are computed both by using Equation (5) directly (solid lines), and also by first projecting the flow onto a TG basis and then using Equation (5) (dashed lines) – the zonal pressure terms are left unchanged by this projection, which does not affect the results of Figure 2. As seen above with the pressure spectra (Figure 1, bottom), the estimate of the pressure variations is modified by the projection, but typically not by more than the difference between the flow models. This shows that calculating the pressure on the basis of the formalism by GL90, even for a flow model that does not strictly obey the TG constraint, is not a source of errors significantly larger than the uncertainty connected to the flow models.

Finally we recall that degree-1 pressure changes are also possibly associated with surface deformations. The zonal decadal variations of the degree-1 CMB pressure were computed in Greff-Lefftz & Legros (2007) (see their Figure 5) and were similar in magnitude (50-100 Pa) to those presented in our Figures 2 and 3. The associated displacement of the mantle required to conserve the centre of mass is of the order of 0.2 mm, again similar to the surface displacement for degrees 2 to 4 shown here. In order to link those to degree-1 pressure changes at the inner core surface (and thus to geocenter mo-

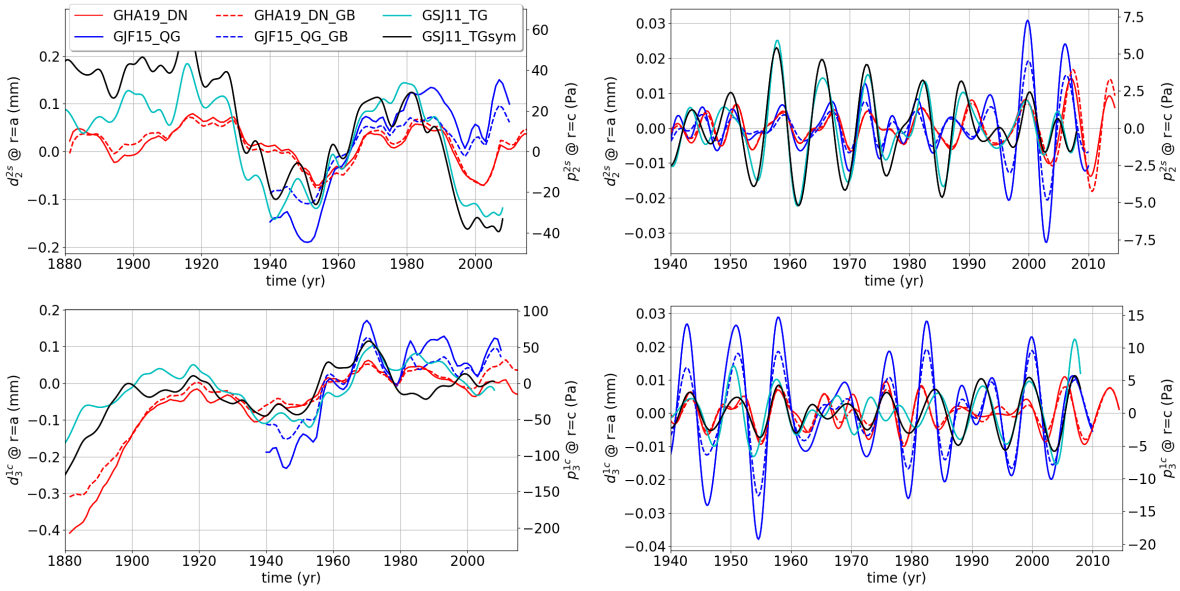

Figure 3. Left: time series of the vertical deformation at the Earth's surface (left y-axis, in mm) for non-zonal coefficients d_2^{2s} (top) and d_3^{1c} (bottom), for the different flow models listed in Table 3. The change in the associated coefficients of pressure at the CMB p_2^{2s} and p_3^{1c} is indicated on the right y-axis (in Pa). The extension '_GB' indicates a projection of the flow model onto a TG basis prior to using Equation (5). Right: time series band-pass filtered between 4 and 9.5 yr. The legend is common to all 4 panels.

tions), one would need to know the force balance in the whole outer core, and thus to use a dynamical model. This is out of the scope of the present study.

4.2.2 Sub-decadal fluctuations

To focus on a possible 6-yr signal of core origin, as put forward by Ding & Chao (2018) and Watkins et al. (2018), we investigate interannual deformations contained in the time-series of the coefficients $d_n^{mc,s}$. We band-pass filter the series for periods between 4 and 9.5 yrs, using a causal Butterworth filter of order 4. For the coefficients shown in Figures 2 and 3, their filtered time-series are shown in the right panels. There are important differences between the predictions from the different flow models, notably the amplitude of non-zonal coefficients can differ by as much as a factor of 2. The amplitude of each individual coefficient of the CMB pressure and vertical deformation at interannual periods, zonal or non-zonal, are smaller than 20 Pa and 0.04 mm, respectively. This is more than 40 times smaller than the 1.7 mm signal of the degree-2 order-2 coefficient found at the 6 yr period by Ding & Chao (2018), and 25 times smaller than the 1 mm signal suggested by Watkins et al. (2018).

At interannual periods, zonal flows are of the order of 0.4 km yr^{-1} (Gillet et al. 2010, 2015b). In comparison, non-zonal flows in the same frequency band can reach locally amplitudes up to a

few km yr^{-1} (e.g. Gillet et al. 2015b; Kloss & Finlay 2019). However, such changes involve smaller length-scale flows associated with harmonic degrees $n > 3$. These have a negligible impact on surface deformations because of the rapid decrease with n of the Love number h_n (see Figure 1). Interannual changes in individual non-zonal flow coefficients of spherical harmonic degree 2 or 3 are not larger than approximately 0.2 km yr^{-1}, of similar amplitude than the zonal flow coefficients. Hence, this is why the non-zonal low degree coefficients of the surface deformation (e.g. d_2^{2s} as shown in Figure 3) are of similar amplitude than the zonal coefficients (e.g. d_2^0 as shown in Figure 2).

From $\hat{d}_n^{mc,s}(f)$ the Fourier transform of $\tilde{d}_n^{mc,s}(t)$, we estimate the r.m.s. power of the vertical deformation at the Earth's surface, as a function of frequency f:

$$P_d(f) = \sum_n \frac{1}{2n+1} \sum_{m=1}^{n} \left[\hat{d}_n^0(f)^2 + \sum_{m=1}^{n} \left(\hat{d}_n^{mc}(f)^2 + \hat{d}_n^{ms}(f)^2 \right) \right] . \tag{18}$$

It is represented in Figure 4 for each of our flow models. We also show on the same Figure the median power spectrum computed from 63 GPS stations that cover a time span longer than 18 yr. The acronyms for these stations are listed in Table 4. Residual time-series were processed following the IERS2010 Conventions (IERS Conventions 2010) as defined within the International GNSS Service, so that the largest geophysical contributions (solid and oceanic tides, atmospheric loading, polar motion, co-seismic offsets) and instrumental corrections (tropospheric delays, antenna phase shifts,...) were removed. Only hydrological and ice mass loading and other unmodeled geophysical deformation signals, like processes in the Earth's deep interior, may remain in the datasets. We refer to the paper by Rebischung et al. (2016) for details on the GPS processing strategies and accuracy.

The power of the deformations induced by core flows is many orders of magnitude smaller than the power observed at GPS stations. In the vicinity of 6 years, the r.m.s. deformation over the Earth surface is only approximately 0.01 mm, two orders of magnitude weaker than that invoked by Ding & Chao (2018) for the degree-2, order-2 contribution. Contrary to the rather flat power found for observed series, the power predicted for core induced deformations decreases rapidly towards short periods, in connection with the red spectrum of core motions (shorter periods carry less power, see Gillet et al. 2015b). The power spectrum indicates that, for deformation induced by core motions, millimetric amplitudes may only be achieved at periods much longer than the available GPS records to date.

ALBH	ALGO	ALIC	AREQ	AUCK	BOR1	BRMU	CAS1	COCO	CRO1
DAV1	DRAO	FAIR	GODE	GOLD	GOPE	GRAS	GRAZ	GUAM	HERS
HOB2	HOLB	JOZE	JPLM	KARR	KERG	KIRU	KOKB	KOUR	LAMA
MAC1	MAS1	MATE	MAW1	MCM4	METS	MONP	NANO	NYAL	ONSA
OUSD	PERT	PIE1	POL2	POTS	QUIN	REYK	SANT	SFER	STJO
SYOG	TABL	TIDB	TSKB	UCLU	USUD	VILL	VNDP	WES2	WILL
WTZR	YELL	ZIMM							

Table 4. List of the 63 GPS stations that cover a time span longer than 18 yr (produced by the International GNSS Service; Rebischung et al. 2016) and used to produce Figure 4.

5 DISCUSSION

5.1 The limited topography changes from outer core dynamics

We have shown here that decadal changes in core flows lead to pressure changes of the order of 50-100 Pa at the CMB. The mechanical deformation in the whole Earth induced by this pressure change lead to vertical deformations at the Earth's surface of the order of 0.3 mm. At interannual periods, the CMB pressure change and surface displacement are an order of magnitude smaller, approximately 5-10 Pa and 0.03 mm, respectively. These estimates apply only to the low spherical harmonic degrees

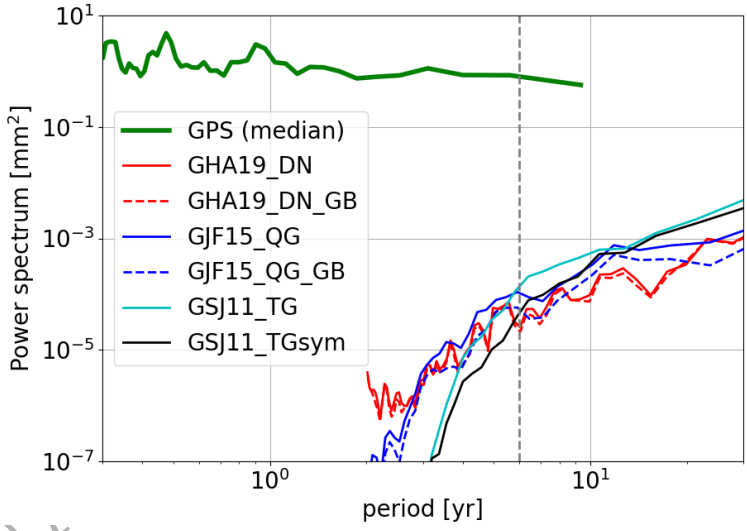

Figure 4. Power spectra of deformation series at the Earth's surface, in mm^2. In bold green the median power spectrum level taken over the set of 63 GPS stations (from the International GNSS Service) covering a time-period longer than 18 yr (see Table 4). Other series represent the r.m.s. power at the Earth's surface, as defined in Equation (18), for predictions from the several core surface flow models listed in Table 3. The vertical dotted line indicates the 6-yr period.

2 or 3; the amplitude of the predicted changes at smaller length scales decrease rapidly with increasing harmonic degree.

The specific time history of the vertical deformation at a given point at the Earth's surface depends sensitively on the choice of the core flow model. However, it is difficult to conceive how using different flow models than the ones we have considered in our study could drastically change the typical amplitudes that we have retrieved; ultimately, all flow models are built to fit the observed secular variation of the magnetic field.

We have focused our efforts here on elastic deformations resulting from pressure variations at the CMB. In addition to those, temporal variations in density anomalies within the volume of the fluid core lead to global changes in the gravity field, which induce further elastic deformations. Although these density anomalies are very small (of the order of $2\rho\Omega U/g \sim 7\times10^{-5}$ kg m^{-3}, based on a balance involving Coriolis and buoyancy forces, with the numerical values of Table 2 and $U \sim 5\times10^{-4}$ m s^{-1}), their integration over the large volume of the core can nevertheless lead to changes in the gravity field that are comparable to those associated with CMB pressure changes (Dumberry 2010). Temporal changes in the density field within the core should then contribute to an additional surface deformation. However, this contribution tends to be opposite to that from CMB pressure changes (Dumberry 2010). Hence, the surface deformation predictions that we have presented are likely overestimated.

In the light of our results, we must conclude that core flows cannot be responsible for the ~ 1 mm amplitude, 6 yr signals in surface deformation extracted from GPS data by Ding & Chao (2018) and Watkins et al. (2018). In order to generate a 1 mm surface deformation, pressure changes at the CMB would need to be increased by a factor 20 to 40, implying a similar factor of increase in the amplitude of core flows at interannual periods. Since flow models are consistent with the observed geomagnetic field variation, the latter is then incompatible with a millimetric interannual surface deformation from core origin.

5.2 The lack of evidence for a connection between surface deformations and geomagnetic field changes

The study of Ding & Chao (2018) in particular argues in favor of a core origin for a degree 2, order 2 GPS signal travelling westward, completing a half rotation of the Earth in 6 yr. Their argument stems from a similar signal which they claim to observe in geomagnetic observatory data, with amplitudes of 8.9 nT and 4.0 nT in the vertical and horizontal components, respectively. However, Gauss coefficient time series for the geomagnetic field of core origin show no distinctive spectral lines at interannual periods (Lesur et al. 2018). Moreover, as we argue above, in order to be compatible with a ~ 1 mm amplitude vertical displacement, the geomagnetic variation would need to be much larger.

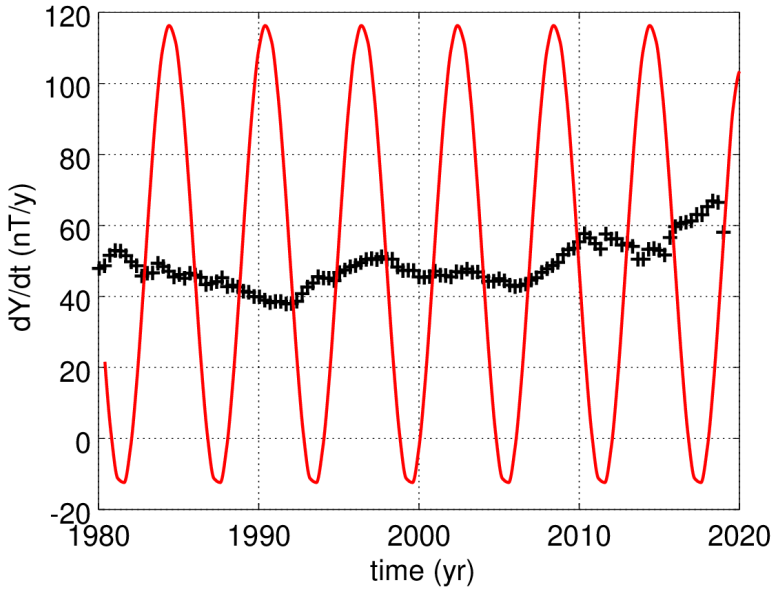

Figure 5. Eastward component of the rate of change of the magnetic field, dY/dt, at the ground-based observatory of Chambon-la-Forêt in France (in nT yr^{-1}): annual difference of 4-monthly means (black crosses), and prediction (red solid line) for a core surface flow determined by equation (19) – see text for details.

In order to illustrate this latter point more explicitly, let us consider a westward propagating wave at the CMB generating a degree 2, order 2 pressure change with frequency $\omega = 2\pi/6$ yr^{-1}. The simplest set of TG core flow coefficients that can generate such a pressure is (see GL90, equations 4b and 4d)

$$\begin{cases} s_2^{2c} = \hat{A}\cos(\omega t)\,, & s_2^{2s} = -\hat{A}\sin(\omega t) \\ t_3^{2c} = -\hat{A}b_2^2\sin(\omega t)\,, & t_3^{2s} = -\hat{A}b_2^2\cos(\omega t) \end{cases}, \tag{19}$$

where $b_2^2 \simeq 1.789$ (given by equation 5b in GL90). The amplitude $\hat{A} = 3.45$ km yr^{-1} is chosen such that it generates a vertical surface deformations with an amplitude of 1 mm. We build a prediction of the global secular variation (or rate of change) of the geomagnetic field that would result from such a wave by time-stepping the radial induction equation at the core surface with a flow specified by Equation (19). For the radial magnetic field at the CMB, we use the CHAOS-6 field model of Finlay et al. (2016) in 2015. Figure 5 shows a comparison between this prediction and the observed secular variation for the Eastward (dY/dt) component at the Chambon-la-Forêt observatory in France. As expected, the amplitude of the secular variation associated with the required pressure wave is more than one order of magnitude larger than that recorded in magnetic observatories. Carrying this exercise at other magnetic observatories and also for the North (dX/dt) and vertical (dZ/dt) components of the secular variation does not alter this general conclusion.

5.3 Gravity field variations induced by core processes

5.3.1 Gravity changes induced by fluid motions at the core surface

We focused our efforts on the role that core flows play in the deformation at the Earth's surface. But we can also asses their contribution to changes in the gravitational potential. Changes in the Stokes coefficients ΔC_{nm} and ΔS_{nm} are directly connected to the pressure coefficients at the CMB (see Equations (14-15) of Dumberry 2010),

$$\left(\Delta C_{nm}, \Delta S_{nm}\right) = \frac{k_n}{\sqrt{2n+1}} \frac{a}{GM\bar{\rho}} \left(p_n^{mc}, p_n^{ms}\right), \tag{20}$$

with G the gravitational constant and M the mass of Earth (numerical values are given in Table 2). k_n is a gravity Love number. For degree 2, $k_2 = 0.1116$ (DB04, GPL04), and a typical change in p_2^2 of 50 Pa at decadal periods (see Figure 3, left) leads to variations of the order of 4×10^{-12} in Stokes coefficients of degree 2, consistent with the results of Dumberry (2010). This is an order of magnitude smaller than the observed variations (of the order of 5×10^{-11} for solutions by Cox et al. 2003). The k_n Love numbers decrease rapidly with increasing n, so changes in Stokes coefficients from core flows decrease rapidly for higher harmonic degrees. Focusing on interannual periods, with a change in p_2^2 of amplitude 4 Pa (see Figure 3, right), changes in Stokes coefficients of degree 2 are of the order of $\Delta C_{22} = 3 \times 10^{-13}$. To give a sense of the associated amplitude in gravity variation, at a point on the equator, this corresponds to a maximum gravity change of $\Delta g = 2g\gamma\Delta C_{22} = 1$ ngal, where the factor $\gamma = 3\sqrt{5/12}$ comes from the normalization of the associated Legendre polynomial. The equivalent change in geoid height is $a\gamma\Delta C_{22} = 0.004$ mm.

These estimates are useful in the context of the suggestion by Mandea et al. (2012) that an interannual variation in the gravity field of a few hundred ngal in the equatorial region of the Atlantic is of core origin. This is 2 orders of magnitude larger than our above estimate for a signal deduced from core flows models. Moreover, the gravity signal emphasized by Mandea et al. spreads over a limited area at the Earth's surface. It is thus associated with larger harmonic degrees, requiring core flows of even larger magnitude. The correlation between geomagnetic and gravity fluctuations highlighted by Mandea et al. (2012) would then just be a coincidence. Core surface motions being too weak to explain observed interannual changes in the Earth gravity field and deformations, alternative processes must be envisionned, either deep in the core (e.g. dissolution/cristallization at the CMB, see Mandea et al. 2015) or at the Earth's surface. We analyse below another possibility in link with the density contrast at the inner core boundary (ICB).

5.3.2 Gravity changes associated with an oscillating inner core

An additional contribution to gravity variations is from azimuthal oscillations of the inner core. The topography of the ICB (of radius $b = 1220$ km) should feature a degree-2 variation along the equator, as the ICB coincides with an equipotential surface that must align with the gravitational potential from the degree-2, order-2 mass anomalies imposed by the mantle (e.g Buffett 1996). An azimuthal rotation of the inner core thus produces a density perturbation of degree and order $(n, m) = (2, 2)$, and an associated gravity variation.

To estimate the amplitude of this contribution, let us choose an equilibrium ICB topography with a maximum in $\phi = 0$. Expressed in terms of equivalent surface mass density $\sigma_{22}(t)$, they are connected to temporal change in $\Delta S_{22}(t)$ by

$$\Delta S_{22} = (1 + \kappa)\frac{4\pi}{\sqrt{5}}\frac{b^4}{Ma^2}\sigma_{22}(t)\,, \tag{21}$$

where we have used Equations (1), (5) and (7) from Dumberry (2010). The factor $(1 + \kappa)$, with $\kappa \simeq 0.97$, accounts for elastic deformations of the Earth associated with a density change at the ICB (Dumberry 2008).

Note that the prediction from Equation (21) assumes an elastic inner core rheology. If the characteristic timescale of viscous deformation (τ) within the inner core is of the same order or smaller than the oscillation period, the ICB topography relaxes back toward its equilibrium alignment with the mantle. Assuming a Maxwell rheology, the right-hand side of Equation (21) would need to be multiplied by a factor $\exp[-t/\tau]$. The viscosity of the inner core is not known so it is difficult to constrain τ. Yet, inferences from high-pressure experiments (e.g. Gleason & Mao 2013), first-principle calculations (e.g. Ritterbex & Tsuchiya 2020) and geodynamics (e.g. Buffett 1997; Greff-Lefftz et al. 2000; Koot & Dumberry 2011; Davies et al. 2014) all point to a weak inner core with τ likely smaller than a decade. The prediction from Equation (21) then represents an upper bound of the possible gravity signal associated with an inner core oscillation.

For an azimuthal oscillation $\phi(t) = \phi_o \sin(\omega t) \ll 1$, of longitudinal amplitude ϕ_o and frequency ω, the temporal surface mass density variation is, for a pattern of spherical harmonic order $m = 2$,

$$\sigma_{22}(t) = h_{22}\Delta\rho \sin(2\phi(t)) \simeq 2h_{22}\Delta\rho\,\phi_o \sin(\omega t)\,. \tag{22}$$

Here $\Delta\rho$ is the density contrast between the inner core and fluid core (about 600 kg m^{-3}, see Gubbins et al. 2008; Tkalčić et al. 2009), and h_{22} is the coefficient of the degree-2, order-2 ICB topography. Undulations of the degree-2 geoid at the CMB are of the order of 50 m (see for instance Fig. 1 in Čadek & Fleitout 2006). For a potential of degree 2 imposed at the CMB, its amplitude inside the core is proportional to the radius. Hence, we estimate undulations h_{22} of the geoid at the ICB to be ≈ 15 m.

The amplitude of the azimuthal velocity at the inner core equator associated with the above oscillations is $v_\phi^{icb}(b) = b\omega\phi_o$. We lack a complete understanding of the fluid-solid interaction at the ICB (see Mound & Buffett 2005; Jault & Légaut 2005). Nevertheless, the typical zonal velocity of the fluid close to $r = b$ should be similar to $v_\phi^{icb}(b)$, because the inner core is electromagnetically coupled to the fluid outer core (e.g. Gubbins 1981). We do not have a direct access to the fluid flow just above the ICB, but magnetic data give us access to the flow at the CMB. How these two are related depends on the timescale of the fluctuations. On interannual periods (approximately the Alfvén time T_A), zonal motions are likely invariant along the rotation axis (Jault 2008; Gillet et al. 2011); one example of such case consists of torsional waves transmitted inside the tangent cylinder (Jault & Légaut 2005; Teed et al. 2015). On significantly longer periods a thermal wind balance is expected within the tangent cylinder (Olson & Aurnou 1999), implying gradients along the rotation axis. This is confirmed by geodynamo numerical simulations. These suggest the zonal flow near the ICB is much weaker than that present in the polar caps at the CMB – see Fig. 7 of Schaeffer et al. (2017) and Fig. 5 of Aubert (2019).

At a period of 30 yr ($\omega = 2\pi/30$ yr^{-1}), azimuthal flows in the vicinity of the tangent cylinder at the core surface are about 2 km yr^{-1} (see Gillet et al. 2019, Fig. 12). Assuming invariant flows along the rotation axis, this corresponds to an oscillation amplitude of $\phi_o \approx 8 \times 10^{-3}$ rad, or $\approx 0.4^\circ$. Taking $h_{22} = 15$ m and $\Delta\rho = 600$ kg m^{-3}, we obtain a change in σ_{22} of ≈ 150 kg/m^2, and an associated change of $\Delta S_{22} \approx 1.5 \times 10^{-11}$. One would obtain weaker values if the velocity gradient along the rotation axis is important within the tangent cylinder. For a period of 6 yr, and taking a typical zonal flow amplitude of 0.4 km yr^{-1} (see Gillet et al. 2019, Fig. 11), we get $\phi_o \approx 3 \times 10^{-4}$ rad or 0.018°, $\sigma_{22} \approx 5$ kg m^{-2} and $\Delta S_{22} \approx 5 \times 10^{-13}$. At interannual periods, the gravity change associated with an oscillating inner core are only about twice that from dynamical pressure variations at the CMB. It follows that subdecadal gravity variations associated with inner core oscillations are not likely to be detected geodetically. At decadal periods, the gravity variation of degree 2, order 2 induced by inner core oscillations is potentially larger than that associated with pressure variations near the CMB, with an amplitude approaching that of geophysical records (Cox et al. 2003). This suggests it might eventually be possible to extract this signal from long term gravity observations. However, this will only be possible provided (i) the axial velocity gradient within the tangent cylinder remains weak on decadal periods, (ii) decadal signals due to surface processes are adequately modeled, and (iii) the viscous relaxation timescale of the inner core is longer than a decade.

Chao (2017) has argued for a much larger interannual inner core oscillation amplitude of $\phi_o \approx 0.23^\circ$ if the observed 6 yr LOD change is connected to an exchange of angular momentum between the inner core and the mantle. This would correspond to an estimated change in Stokes coefficients of

$\approx 7 \times 10^{-12}$, more than 10 times larger than our estimate above. However, there are several objections to such a scenario. First, the prediction of the 6 yr LOD changes reconstructed from core flows matches well the observed LOD (Gillet et al. 2010, 2015b). This shows that the angular momentum exchange is dominantly between the mantle and the fluid core (and not between the mantle and the inner core with the fluid core playing a passive role, as assumed by Chao 2017). Second, by electromagnetic coupling, azimuthal inner core oscillations should entrain equally large azimuthal oscillations of the fluid core inside the tangent cylinder (Mound & Buffett 2003, 2006; Jault & Légaut 2005; Dumberry & Mound 2010). Not only this would reduce the amplitude of the oscillation (as it is the whole tangent cylinder that is involved in the oscillation, not just the inner core); the zonal flows at the CMB associated with this oscillation would also be of the order of several km yr^{-1} at the period of 6 yr. These would leave a clear signature in geomagnetic observations, a signature which is not observed.

5.4 Earth's oblateness and length-of-day changes

Although the Earth is subject to external torques (for instance the tidal breaking effect, mainly from the Moon), LOD changes result from the conservation of angular momentum between the solid Earth and its fluid regions (Gross 2015). This involves changes either in the motions within the fluid layers, or in the moment of inertia. Interannual LOD variations on time-scales shorter than 5 yr are primarily explained by atmospheric angular momentum changes, with smaller contributions from hydrological and oceanic processes (e.g. Gross et al. 2004; Chen et al. 2019). From decadal down to about 5 yr periods, LOD variations corrected for tides and atmospheric angular momentum are at first order explained by velocity changes in the fluid core (e.g. Gillet et al. 2019, Fig. 9 and 10). The core angular momentum results primarily from changes in flow coefficients t_1^0 and t_3^0 (see Jault & Finlay 2015). LOD variations ΔT^{cm} induced by core fluid motions can thus be associated to changes in the p_2^0 pressure field at the CMB through (DB04, equations 57 and 58):

$$\Delta T^{cm} = -\frac{I_c}{I_m} \frac{3\pi p_2^0}{\rho \Omega^3 c^2} \,. \tag{23}$$

One may wonder how much global deformations induced by the fluid flow pressure at the CMB may affect the Earth's moment of inertia and the associated changes in the Earth's oblateness $\Delta J_2 = -\sqrt{5}\Delta C_{20}$, related to LOD variations.

On long time-scales, ΔJ_2 are mostly governed by post-glacial rebound and the melting of ice-sheets. At decadal periods have been detected in particular a signal of period 18.6 yr, in link with lunar orbit precession (though still requiring improved theoretical models, see Cheng et al. 2013; Chao et al. 2020), and variations of period about 10.5 yr, not yet convincingly explained by global circulation models (Cheng & Ries 2018). On shorter interannual periods, processes associated with surface fluid

envelopes dominate (e.g. Cheng & Tapley 2004; Meyssignac et al. 2013; Cheng & Ries 2018; Chao et al. 2020). Because Earth's angular momentum must be conserved, a change in the Earth's oblateness is associated with a change in the day length $T = 2\pi/\Omega$. A first order approximation (supposing the core and the mantle decoupled) gives the relation (see Mignard 1986)

$$\Delta T_{J_2} = \frac{4\pi M a^2 \Delta J_2}{3\Omega(I_m + I_c)} \,. \tag{24}$$

Global deformations of the mantle induced by changes in the p_2^0 fluid pressure field at the CMB should then modify the Stokes coefficient C_{20} and thus lead to ΔJ_2. Combining the above relation (23) with equation (52) of DB04, changes in J_2 associated with the global elastic response to p_2^0 are

$$\Delta {J_2}^p = \frac{a p_2^0}{GM} \left[-\frac{k_2}{\overline{\rho}} + \frac{k_m}{\rho} \frac{I_c}{I_m} \frac{a^2}{c^2} \right] , \tag{25}$$

with $k_m = 0.2345$. The second term on the r.h.s. of equation (25) results from the change in centrifugal potential, which depends on ΔT^{cm}. Its magnitude is about one half that of the term in k_2. 50 Pa changes in p_2^0 at decadal periods result in $\Delta {J_2}^p \approx 8 \times 10^{-12}$. This is significantly weaker than unexplained changes in J_2 seen at 10.5 yr and 18.6 yr periods, of amplitude respectively $\approx 10^{-10}$ and 4×10^{-11} (residuals after removing seasonal, tidal and long trend components, see Chao et al. 2020).

Finally, combining equations (24) and (25), we estimate LOD changes induced by p_2^0 variations through global elastic deformations to

$$\Delta T_{{J_2}^p} = \frac{4\pi a^3 p_2^0}{3G\Omega(I_m + I_c)} \left[-\frac{k_2}{\overline{\rho}} + \frac{k_m}{\rho} \frac{I_c}{I_m} \frac{a^2}{c^2} \right] . \tag{26}$$

This gives $\Delta T_{{J_2}^p} \approx 1.5 \times 10^{-3}$ ms for 50 Pa changes in p_2^0 at decadal time scales, and $\approx 10^{-4}$ ms for 4 Pa changes at interannual periods (see Figure 2). This is by far smaller than LOD changes ΔT^{cm} resulting from core motion (respectively of the order of 1 ms and 0.2 ms at decadal and interannual periods), and thus negligeable. It is also much less than the contribution to the LOD from changes in the moment of inertia of surface envelopes. Indeed, Cheng & Ries (2018) indicate interannual variations in J_2 of the order of 10^{-10}, which from (24) corresponds to a LOD change $\Delta T_{J_2} \approx 0.015$ ms.

6 CONCLUSION

To conclude, planetary scale elastic deformations of the Earth in response to changes in the dynamical pressure from core motions near the CMB are likely below the uncertainty level of GNSS observations at present-day (e.g. Teferle et al. 2008). Observed interannual changes in the Earth's surface topography require an alternative geophysical explanation. Leaving aside possible but largely undetermined deep processes (e.g Mandea et al. 2015), sub-decadal signals in GNSS time series are likely caused by

the re-distribution of continental water (see Gegout et al. 2010; Dill & Dobslaw 2013) as well as other non-tidal surface loading effects associated with climate variability (Meyssignac et al. 2013; Mémin et al. 2015)

ACKNOWLEDGEMENTS

We thank Dominique Jault and David Cébron for constructive discussions on the pressure estimate and mantle deformations. Reviews by R. Gross and M. Greff-Lefftz helped improve the quality of our manuscript. NG was partially supported by the French Centre National d'Etudes Spatiales (CNES) for the study of Earth's core dynamics in the context of the *Swarm* mission of ESA. MD is supported by a Discovery Grant from NSERC/CRSNG. SR acknowledges support by the CNES through the TOSCA program. This project has been funded by ESA in the framework of EO Science for Society, through contract 4000127193/19/NL/IA (SWARM + 4D Deep Earth: Core).

REFERENCES

Alterman, Z., Jarosch, H., & Pekeris, C., 1959. Oscillations of the Earth, *Proc. R. Soc. London. A: Mathematical and Physical Sciences*, **252**(1268), 80–95.

Amit, H. & Olson, P., 2004. Helical core flow from geomagnetic secular variation, *Phys. Earth Planet. Int.*, **147**(1), 1–25.

Aubert, J., 2018. Geomagnetic acceleration and rapid hydromagnetic wave dynamics in advanced numerical simulations of the geodynamo, *Geophys. J. Int.*, **214**(1), 531–547.

Aubert, J., 2019. Approaching Earth's core conditions in high-resolution geodynamo simulations, *Geophys. J. Int.*, **219**(1), S137–S151.

Aubert, J., Gastine, T., & Fournier, A., 2017. Spherical convective dynamos in the rapidly rotating asymptotic regime, *J. Fluid Mech.*, **813**, 558–593.

Baerenzung, J., Holschneider, M., & Lesur, V., 2016. The flow at the Earth's core-mantle boundary under weak prior constraints, *J. Geophys. Res.: Solid Earth*, **121**(3), 1343–1364.

Barrois, O., Gillet, N., & Aubert, J., 2017. Contributions to the geomagnetic secular variation from a reanalysis of core surface dynamics, *Geophys. J. Int.*, **211**(1), 50–68.

Bloxham, J., 1992. The steady part of the secular variation of the Earth's magnetic field, *J. Geophys. Res.: Solid Earth*, **97**(B13), 19565–19579.

Buffett, B., 2014. Geomagnetic fluctuations reveal stable stratification at the top of the Earth's core, *Nature*, **507**(7493), 484–487.

Buffett, B. A., 1996. Gravitational oscillations in the length of the day, *Geophys. Res. Lett.*, **23**, 2279–2282.

Buffett, B. A., 1997. Geodynamic estimates of the viscosity of the earth's inner core, *Nature*, **388**(6642), 571–573.

Čadek, O. & Fleitout, L., 2006. Effect of lateral viscosity variations in the core-mantle boundary region on predictions of the long-wavelength geoid, *Studia Geophysica et Geodaetica*, **50**(2), 217–232.

Chao, B., Yu, Y., & Chung, C., 2020. Variation of earth's oblateness j2 on interannual-to-decadal timescales, *J. Geophys. Res.: Solid Earth*, **125**(6), e2020JB019421.

Chao, B. F., 2017. Dynamics of axial torsional libration under the mantle-inner core gravitational interaction, *J. Geophys. Res.: Solid Earth*, **122**, 560–571.

Chen, J., Wilson, C. R., Kuang, W., & Chao, B. F., 2019. Interannual oscillations in earth rotation, *Journal of Geophysical Research: Solid Earth*, **124**(12), 13404–13414.

Cheng, M. & Ries, J. C., 2018. Decadal variation in earth's oblateness (j 2) from satellite laser ranging data, *Geophys. J. Int.*, **212**(2), 1218–1224.

Cheng, M. & Tapley, B. D., 2004. Variations in the earth's oblateness during the past 28 years, *J. Geophys. Res.: Solid Earth*, **109**(B9).

Cheng, M., Tapley, B. D., & Ries, J. C., 2013. Deceleration in the Earth's oblateness, *J. Geophys. Res.: Solid Earth*, **118**(2), 740–747.

Cox, C., Au, A., Boy, J.-P., Chao, B., Noomen, R., Klosko, S., Noll, C., & Pearlman, M., 2003. Time-variable gravity: Using Satellite-Laser-Ranging as a tool for observing long-term changes in the Earth system, in Proceedings of the 13th International Workshop on Laser Ranging. Greenbelt, MD: NASA Goddard Space Flight Center.

Crossley, D., 1975. The free-oscillation equations at the centre of the Earth, *Geophys. J. Int.*, **41**(2), 153–163.

Davies, C. J., Stegman, D. R., & Dumberry, M., 2014. The strength of gravitational core-mantle coupling, *Geophys. Res. Lett.*, **41**(11), 3786–3792.

Dill, R. & Dobslaw, H., 2013. Numerical simulations of global-scale high-resolution hydrological crustal deformations, *J. Geophys. Res.: Solid Earth*, **118**(9), 5008–5017.

Ding, H. & Chao, B. F., 2018. A 6-year westward rotary motion in the Earth: Detection and possible MICG coupling mechanism, *Earth Planet. Sc. Lett.*, **495**, 50–55.

Dumberry, M., 2008. Decadal variations in gravity caused by a tilt of the inner core, *Geophys. J. Int.*, **172**, 921–933.

Dumberry, M., 2010. Gravity variations induced by core flows, *Geophys. J. Int.*, **180**(2), 635–650.

Dumberry, M. & Bloxham, J., 2004. Variations in the Earth's gravity field caused by torsional oscillations in the core, *Geophys. J. Int.*, **159**(2), 417–434.

Dumberry, M. & Mound, J. E., 2010. Inner core – mantle gravitational locking and the super-rotation of the inner core, *Geophys. J. Int.*, **181**, 806–817.

Dziewonski, A. M. & Anderson, D. L., 1981. Preliminary reference Earth model, *Phys. Earth Planet. Int.*, **25**(4), 297–356.

Fang, M., Hager, B. H., & Herring, T. A., 1996. Surface deformation caused by pressure changes in the fluid core, *Geophys. Res. Lett.*, **23**(12), 1493–1496.

Finlay, C. C. & Jackson, A., 2003. Equatorially dominated magnetic field change at the surface of Earth's

core, *Science*, **300**(5628), 2084–2086.

Finlay, C. C., Olsen, N., Kotsiaros, S., Gillet, N., & Tøffner-Clausen, L., 2016. Recent geomagnetic secular variation from Swarm and ground observatories as estimated in the CHAOS-6 geomagnetic field model, *Earth, Planets and Space*, **68**(1), 112.

Fournier, A., Aubert, J., & Thébault, E., 2011. Inference on core surface flow from observations and 3-D dynamo modelling, *Geophys. J. Int.*, **186**(1), 118–136.

Gegout, P., Boy, J.-P., Hinderer, J., & Ferhat, G., 2010. Modeling and observation of loading contribution to time-variable GPS sites positions, in Gravity, geoid and Earth observation, pp. 651–659, Springer.

Gerick, F., Jault, D., Noir, J., & Vidal, J., 2020. Pressure torque of torsional Alfvén modes acting on an ellipsoidal mantle, *Geophys. J. Int.*, **222**(1), 338–351.

Gillet, N., Pais, M., & Jault, D., 2009. Ensemble inversion of time-dependent core flow models, *Geochem. Geophys. Geosyst.*, **10**(6).

Gillet, N., Jault, D., Canet, E., & Fournier, A., 2010. Fast torsional waves and strong magnetic field within the Earth's core, *Nature*, **465**(7294), 74–77.

Gillet, N., Schaeffer, N., & Jault, D., 2011. Rationale and geophysical evidence for quasi-geostrophic rapid dynamics within the Earth's outer core, *Phys. Earth Planet. Int.*, **187**(3), 380–390.

Gillet, N., Jault, D., Finlay, C., & Olsen, N., 2013. Stochastic modeling of the Earth's magnetic field: inversion for covariances over the observatory era, *Geochem. Geophys. Geosyst.*, **14**(4), 766–786.

Gillet, N., Barrois, O., & Finlay, C. C., 2015a. Stochastic forecasting of the geomagnetic field from the COV-OBS.x1 geomagnetic field model, and candidate models for IGRF-12, *Earth, Planets and Space*, **67**(1), 1–14.

Gillet, N., Jault, D., & Finlay, C., 2015b. Planetary gyre, time-dependent eddies, torsional waves, and equatorial jets at the Earth's core surface, *J. Geophys. Res.: Solid Earth*, **120**(6), 3991–4013.

Gillet, N., Huder, L., & Aubert, J., 2019. A reduced stochastic model of core surface dynamics based on geodynamo simulations, *Geophys. J. Int.*, **219**(1), 522–539.

Gire, C. & Le Mouël, J.-L., 1990. Tangentially geostrophic flow at the core-mantle boundary compatible with the observed geomagnetic secular variation: the large-scale component of the flow, *Phys. Earth Planet. Int.*, **59**(4), 259–287.

Gleason, A. & Mao, W., 2013. Strength of iron at core pressures and evidence for a weak earths inner core, *Nature Geoscience*, **6**(7), 571–574.

Greff-Lefftz, M. & Legros, H., 1997. Some remarks about the degree-one deformation of the earth, *Geophys. J. Int.*, **131**(3), 699–723.

Greff-Lefftz, M. & Legros, H., 2007. Fluid core dynamics and degree-one deformations: Slichter mode and geocenter motions, *Phys. Earth Planet. Int.*, **161**(3-4), 150–160.

Greff-Lefftz, M., Legros, H., & Dehant, V., 2000. Influence of the inner core viscosity on the rotational eigenmodes of the earth, *Phys. Earth Planet. Int.*, **122**(3-4), 187–204.

Greff-Lefftz, M., Pais, M., & Le Mouel, J.-L., 2004. Surface gravitational field and topography changes induced by the Earth's fluid core motions, *Journal of Geodesy*, **78**(6), 386–392.

Gross, R. S., 2015. Earth rotation variations-long period, *Treatise on geophysics*, **3**, 215–261.

Gross, R. S., Fukumori, I., Menemenlis, D., & Gegout, P., 2004. Atmospheric and oceanic excitation of length-of-day variations during 1980–2000, *J. Geophys. Res.: Solid Earth*, **109**(B1).

Gubbins, D., 1981. Rotation of the inner core, *J. Geophys. Res.*, **86**, 11695–11699.

Gubbins, D., Masters, G., & Nimmo, F., 2008. A thermochemical boundary layer at the base of Earth's outer core and independent estimate of core heat flux, *Geophys. J. Int.*, **174**(3), 1007–1018.

Holme, R., 2015. Large scale flow in the core, in Treatise in Geophysics, Core Dynamics, vol. 8, chap. 4, pp. 91–113, eds Olson, P. & Schubert, G., Elsevier.

IERS Conventions, 2010. IERS Technical note 36, p. 179, eds Petit, G. & Luzum, B., Frankfurt am Main: Verlag des Bundesamts für Kartographie und Geodäsie.

Jackson, A., 1997. Time-dependency of tangentially geostrophic core surface motions, *Phys. Earth Planet. Int.*, **103**(3-4), 293–311.

Jault, D., 2008. Axial invariance of rapidly varying diffusionless motions in the Earth's core interior, *Phys. Earth Planet. Int.*, **166**, 67–76.

Jault, D. & Finlay, C. C., 2015. Waves in the core and mechanical core-mantle interactions, in Treatise on Geophysics, Core Dynamics, 2nd edition, vol. 8, chap. 8.09, pp. 225–244, eds Schubert, G. & Olson, P., Elsevier, Oxford.

Jault, D. & Légaut, G., 2005. Alfvén waves within the Earth's core, *Fluid dynamics and dynamos in astrophysics and geophysics*, pp. 277–293.

Kloss, C. & Finlay, C. C., 2019. Time-dependent low-latitude core flow and geomagnetic field acceleration pulses, *Geophys. J. Int.*, **217**(1), 140–168.

Koot, L. & Dumberry, M., 2011. Viscosity of the earth's inner core: Constraints from nutation observations, *Earth Planet. Sci. Lett.*, **308**(3-4), 343–349.

Labbé, F., Jault, D., & Gillet, N., 2015. On magnetostrophic inertia-less waves in quasi-geostrophic models of planetary cores, *Geophys. Astrophys. Fluid Dyn.*, **109**(6), 587–610.

Le Mouël, J., 1984. Outer-core geostrophic flow and secular variation of Earth's geomagnetic field, *Nature*, **311**(5988), 734–735.

Le Mouël, J., Gire, C., & Madden, T., 1985. Motions at core surface in the geostrophic approximation, *Phys. Earth Planet. Int.*, **39**(4), 270–287.

Lesur, V., Wardinski, I., Baerenzung, J., & Holschneider, M., 2018. On the frequency spectra of the core magnetic field Gauss coefficients, *Phys. Earth Planet. Int.*, **276**, 145–158.

Love, A. E. H., 1909. The yielding of the Earth to disturbing forces, *Proc. R. Soc. Lond., A*, **82**, 73–88.

Mandea, M., Panet, I., Lesur, V., De Viron, O., Diament, M., & Le Mouël, J.-L., 2012. Recent changes of the Earth's core derived from satellite observations of magnetic and gravity fields, *Proc. Natl. Acad. Sci. USA*, **109**(47), 19129–19133.

Mandea, M., Narteau, C., Panet, I., & Le Mouël, J.-L., 2015. Gravimetric and magnetic anomalies produced by dissolution-crystallization at the core-mantle boundary, *J. Geophys. Res.: Solid Earth*, **120**(9), 5983–6000.

Mémin, A., Flament, T., Alizier, B., Watson, C., & Rémy, F., 2015. Interannual variation of the Antarctic ice sheet from a combined analysis of satellite gravimetry and altimetry data, *Earth Planet. Sci. Lett.*, **422**, 150–156.

Meyssignac, B., Lemoine, J., Cheng, M., Cazenave, A., Gégout, P., & Maisongrande, P., 2013. Interannual variations in degree-2 Earth's gravity coefficients c_{20}, c_{21} and s_{22} reveal large-scale mass transfers of climatic origin, *Geophys. Res. Lett.*, **40**(15), 4060–4065.

Mignard, F., 1986. Tidal and non tidal acceleration of the earths rotation, in Earth Rotation: Solved and Unsolved Problems, pp. 93–110, Springer.

Mound, J. E. & Buffett, B. A., 2003. Interannual oscillations in the length of day: implications for the structure of mantle and core, *J. Geophys. Res.*, **108(B7)**, 2334, doi:10.1029/2002JB002054.

Mound, J. E. & Buffett, B. A., 2005. Mechanisms of core-mantle angular momentum exchange and the observed spectral properties of torsional oscillations, *J. Geophys. Res.*, **110**, B08103, doi:10.1029/2004JB003555.

Mound, J. E. & Buffett, B. A., 2006. Detection of a gravitational oscillation in length-of-day, *Earth Planet. Sc. Lett.*, **243**, 383–389.

Olson, P. & Aurnou, J., 1999. A polar vortex in the Earth's core, *Nature*, **402**(6758), 170–173.

Pais, M. & Jault, D., 2008. Quasi-geostrophic flows responsible for the secular variation of the Earth's magnetic field, *Geophys. J. Int.*, **173**(2), 421–443.

Rebischung, P., Altamimi, Z., Ray, J., & Garayt, B., 2016. The IGS contribution to ITRF2014, *Journal of Geodesy*, **90**(7), 611–630.

Ritterbex, S. & Tsuchiya, T., 2020. Viscosity of hcp iron at earths inner core conditions from density functional theory, *Scientific reports*, **10**(1), 1–9.

Schaeffer, N. & Cardin, P., 2005. Quasigeostrophic model of the instabilities of the Stewartson layer in flat and depth-varying containers, *Phys. Fluids*, **17**(10), 104111.

Schaeffer, N., Jault, D., Nataf, H.-C., & Fournier, A., 2017. Turbulent geodynamo simulations: a leap towards Earth's core, *Geophys. J. Int.*, **211**(1), 1–29.

Teed, R. J., Jones, C. A., & Tobias, S. M., 2015. The transition to Earth-like torsional oscillations in magneto-convection simulations, *Earth Planet. Sci. Lett.*, **419**, 22–31.

Teferle, F. N., Williams, S. D., Kierulf, H. P., Bingley, R. M., & Plag, H.-P., 2008. A continuous GPS coordinate time series analysis strategy for high-accuracy vertical land movements, *Physics and Chemistry of the Earth, Parts A/B/C*, **33**(3-4), 205–216.

Tkalčić, H., Kennett, B. L., & Cormier, V. F., 2009. On the inner-outer core density contrast from PKiKP/PcP amplitude ratios and uncertainties caused by seismic noise, *Geophys. J. Int.*, **179**(1), 425–443.

Watkins, A., Fu, Y., & Gross, R., 2018. Earth's subdecadal angular momentum balance from deformation and rotation data, *Scientific Reports*, **8**(1), 13761.